Morphology and evolution of submarine canyons on the northwest South China Sea margin

Shuang Li [a, b, c], Tiago M. Alves [d], Wei Li [a, b, c]*, Xiujuan Wang [e, f], Michele Rebesco [g], Jian Li [a, b, c], Fang Zhao [a, b, c], Kaiqi Yu [a, b, c], Shiguo Wu [c, h]

[a] CAS Key Laboratory of Ocean and Marginal Sea Geology, South China Sea Institute of Oceanology, Chinese Academy of Sciences, Guangzhou 510301, P.R. China

[b] Southern Marine Science and Engineering Guangdong Laboratory (Guangzhou), 511458, P.R. China

[c] University of Chinese Academy of Sciences, Beijing 100049, P.R. China

[d] 3D Seismic Lab, School of Earth and Ocean Sciences, Cardiff University, Main Building, Park Place, Cardiff, CF10 3AT, United Kingdom

[e] Center for Ocean Mega-Science, Key Laboratory of Marine Geology and Environment & Center of Deep-Sea Research, Institute of Oceanology, Chinese Academy of Sciences, Qingdao 266071, China

[f] Laboratory for Marine Mineral Resources, Pilot National Laboratory for Marine Science and Technology (Qingdao), Qingdao 266071, China

[g] Istituto Nazionale di Oceanografia e di Geofisica Sperimentale (OGS), Borgo Grotta Gigante 42/C, Sgonico, 34010 Trieste, Italy

[h] Institute of Deep-sea Science and Engineering, Chinese Academy of Sciences, Sanya, 572000, China

Corresponding author: Dr. Wei Li (wli@scsio.ac.cn)

Abstract

Submarine canyons are widely observed along both passive and active continental margins, but the factors controlling their complex morphology are still poorly understood. Here, we use high-resolution multibeam bathymetric and 2D seismic data to investigate an area of the northwest South China Sea where 48 submarine canyons are identified. These previously unstudied submarine canyons incise the continental shelf and are located at a water depth between 200 m and 2200 m.

Canyon morphology varies from southwest to northeast, namely in what their length and incision depth are concerned. We therefore divide these canyons into four main types: a) Type A, B and C showing a predominant NW-SE direction, and b) Type D canyons striking to the north. By analysing their internal architectures, we propose that submarine canyons along the northwest South China Sea margin were initiated in the Late Miocene by retrogressive slope failure in response to the gradual build-up of sediment on the continental slope. Differences in sediment supply and fault activity are recognised here as the main factors controlling the morphology of the investigated submarine canyons. In addition, recurrent mass-transport deposits (MTDs) fed sediment from the northwest South China Sea margin into the study area, accelerating the filling of the Central Canyon system, a giant submarine canyon located to the south of the investigated continental slope. The discovery of gas fields (LS22-1, LS17-2) and a gas hydrate drilling zone (GMGS5) in the Central Canyon system proves that MTDs comprise good hydrocarbon reservoirs. Our results contribute to a better understanding of the origin and development of submarine canyons and highlight the role of sediment supply and tectonic events in controlling canyon morphology.

Keywords: South China Sea; continental margin; Qiongdongnan Basin; submarine canyons; seafloor morphology.

1 Introduction

Submarine canyons are one of the most common geomorphological features on both passive and active continental margins (Canals et al., 2006; Harris and Whiteway, 2011). They act as the primary conduits for sediment delivered from the continental shelf and upper slope to deep-water sedimentary basins (Puig et al., 2003; de Stigter et al., 2011). In the past two decades, considerable attention has been given to submarine canyons as their sandy infillings can form major petroleum reservoirs (Jobe et al., 2010; Gong et al., 2011; Mansurbeg et al., 2012; Lo Iacono et al., 2014; Tournadour et al., 2017). Coarse-grained material transported by submarine canyons can also form submarine fans with significant hydrocarbon accumulations (Curray et al., 2002; Covault et al., 2007; Zhu et al., 2012).

The initiation and development of submarine canyons is generally related to eroding, downslope-driven sediment flows (Baztan et al., 2005), or to widespread erosion promoted by retrogressive slope failure (Harris and Whiteway, 2011; Krastel et al., 2011). Regardless of their geneses, submarine canyons persist over geological time periods, providing critical sedimentological and climatic information on the evolution of continental margins (Gingele et al., 2004; Zhu et al., 2010). Additionally, detailed morphological investigations of submarine canyons may prevent geohazards when placing submarine infrastructure, such as cables and pipelines, on the seafloor (Lo Iacono et al., 2011).

Submarine canyons have been widely documented in the South China Sea. Key examples are the Pearl River Canyon (Ding et al., 2013; Wang et al., 2014; Li et al., 2019), the Central Canyon system (Gong et al., 2011; Su et al., 2014; Li et al., 2017), the Shenhu Submarine Canyon System (Zhu et al., 2010; Ma et al., 2015; Qiao et al., 2015; Su et al., 2020) and the Taiwan Canyon (Ding et al., 2010; Xu et al., 2014; Li et al., 2021). Ding et al. (2013) and Wang et al. (2014) have investigated the morphology and evolution of the Pearl River Canyon to consider tectonic activity as exerting an important control on its evolution, while Li et al. (2019) investigated the widespread seafloor undulations associated with this canyon and their importance to regional geohazard assessments. By using 2D/3D seismic and well data, Gong et al (2011) have documented the internal architecture and depositional processes of the Central Canyon system to identify four cut-and-fill stages in its interior.

Li et al (2013) also investigated the morphology, sedimentary features and evolution of the Central Canyon system and considered it to have been initiated in the Late Miocene (5.5 Ma). Su et al. (2014) proposed that the morphology of the western part of the Central Canyon system is controlled by sediment supplied from the continental slope to the south, with its eastern segment being influenced by tectonic movements. In addition, a growing number of studies have focused on the morphology, origin and evolution of the Shenhu Submarine Canyon System on the continental slope of Pearl River Mouth Basin. Zhu et al. (2010) proposed that the thermohaline intermediate water circulation of the South China Sea caused the migration of Shenhu Submarine Canyon System after the Middle Miocene. These submarine canyons are considered to reflect the interaction between downslope gravity flows and along-slope bottom currents (Gong et al., 2013; Gong et al., 2018). Based on 2D and 3D seismic data, Ma et al. (2015) proposed that local faulting and sediment supply control the evolution of submarine canyons in the Pearl River Mouth Basin. However, little information is available on the morphology and evolution of submarine canyons on the northwest South China Sea margin.

In this study, we focus on the submarine canyons developed along the northwest South China Sea margin, southeast of Hainan Island (Fig. 1). He et al. (2013) have investigated the surrounding submarine channels and canyons, suggesting the interaction of the along-canyon turbidity currents and bottom currents led to their lateral migration. However, forty-eight (48) submarine canyons at water depths between 200 and 2000 m are still poorly studied on this area (Fig. 2). We investigate the shelf-margin architecture in different sectors of the northwest South China Sea margin, with canyon morphology changing gradually along the continental margin (Figs. 2 and 3), making use of high-resolution multibeam bathymetric data and 2D seismic data. Hence, the specific aims of this study are: (a) to analyse the detailed morphology and internal character of these 48 submarine canyons; (b) to investigate their origin and evolution throughout the Late Miocene; (c) to reveal the factors controlling canyon morphology at a regional scale; and (d) to discuss the links between these 48 submarine canyons and a giant, submarine canyon system (the Central Canyon system) formed immediately south of them.

2 Geological setting

The Qiongdongnan Basin is located in the northwest South China Sea and covers an area of 45,000 km^2 (Shi et al. 2013). The basin was formed by lithospheric stretching that started in the Paleogene in association with continental rifting of the South China Sea (Ru and Pigott, 1986). It is bounded by the Pearl River Mouth Basin to the east, the Xisha High to the south, and the Yinggehai Basin to the west (Wu et al. 2009). The Qiongdongnan Basin recorded syn-rift tectonics from the Paleocene to the Early Oligocene, continental breakup spanning the Late Oligocene to the end of the Middle Miocene, and a post-rift stage between the Late Miocene and the Quaternary (Xie et al., 2006). The post-rift stage can be further split into thermal subsidence and accelerated subsidence sub-stages (Wu et al., 2008).

The study area is located in the central part of the Qiongdongnan Basin at a water depth ranging from 200 m to 2000 m, with the Red River Fault Zone to the west, No.2 fault to the north and the Central Canyon to the south (Fig. 1). The Red River Fault Zone has witnessed three deformation phases; sinistral movement from ~ 30 to 16 Ma, a transitional phase between 16 and 5.5 Ma, and dextral movement after 5.5 Ma (Zhu et al., 2009). The No.2 fault, extending over 460 km in the central part of the Qiongdongnan Basin, was formed in the Late Eocene and its strike changed from ENE to E-W (Ren et al., 2014). The Central Canyon shows an ‘‘S-shaped’’ geometry (Gong et al., 2011; Li et al., 2013). It is ~425 km long and ~9–30 km wide, with an NE to ENE orientation (Yuan et al., 2009; Su et al., 2014). The Central Canyon was generated at the end of the Miocene (5.5 Ma) and its western and central part are buried under thick sediment (Yuan et al., 2009; Gong et al., 2011; Li et al., 2013; Su et al., 2014).

3 Data and methods

The dataset used in this study consists of high-resolution bathymetry and two-dimensional (2D) seismic profiles. Employing a SeaBeam 2112 multibeam echo-sounder, the bathymetric data were acquired by the Guangzhou Marine Geological Survey, Ministry of Land and Resources in 2008 during a geophysical cruise on board the R/V Hai Yang Liu Hao. The SeaBeam 2112 operated at a main frequency of 12 kHz with a pulse length of 3-20 ms. Full bathymetric swath width comprises 120°, and the depth accuracy is better than 0.5% of the water depth. The horizontal and vertical resolutions of the multi-beam bathymetry data are ~100 m and ~1-3.3 m, respectively.

The 2D seismic data were acquired by the China National Offshore Oil Corporation (CNOOC) in 2005 and 2011, respectively. The seismic data acquired in 2005 were processed to a dominant frequency of 30 Hz, with a vertical resolution of 15-20 m. The seismic data acquired in 2011 have a sampling interval of 1 ms, a bin spacing of 25 m × 12.5 m in the inline and crossline directions, and a dominant frequency of ~45 Hz in the upper seismic sequences. The seismic data were recorded with an air gun array with a total volume of 3875 cubic inch and a towing depth of 6-7 m. The 2D seismic data were collected by 6 km long streamer with 480 channels and processed by a time migration. The original seismic data were interpreted in Geoframe 4.5.

Five seismic sequences have been documented in the published literature. These sequences are the Sanya, Meishan, Huangliu, Yinggehai and Ledong formations (Fig. 4). The sequences are bounded by five seismic-stratigraphic markers of regional extent: Horizons T60, T50, T40, T30 and

T20 (Wu et al., 2009). Three main seismic horizons (T20, T30 and T40) are considered in this study, and are dated as 1.9 Ma, 5.5 Ma and 10.5 Ma, respectively (Fig. 4).

4. Results

4.1 General geomorphology of the northwest South China Sea margin

The shelf edge of the northwest South China Sea shows a change from SW-NE to W-E at a latitude of about 18°30′ N (Figs. 1 and 2). It delimits a S-facing continental slope with a shelf break at a water depth of ~200 m (Fig. 2). The northwest South China Sea margin is ~350 km long and shows a nearly graded slope profile (Figs. 5 and 6). The continental slope shows the gentlest gradient in its southwestern part (average of ~3°) and becomes steeper to the northeast, where a maximum gradient of ~23° is observed (Fig. 5). The shelf edge to the southwest is marked by sediment progradation and exhibits a flat to slightly rising trajectory trend (Figs. 6a and 6b). The shelf edge to the northeast shows an essentially aggradational pattern with a steeply rising trajectory (Fig. 6c).

All northwest South China Sea margin is shaped by submarine canyons that are perpendicular to the shelf edge, incising the continental slope at different depths. These 48 submarine canyons extend for about 7 to 20 km, from the shelf edge to the base of the continental slope, down to water depths of ~2000 m (Fig. 3).

4.2 Submarine canyon morphology

The 48 submarine canyons mapped in the study area are relatively linear and strike perpendicularly to the continental slope (Figs. 3a and 3b). They show diverse morphologies, from southwest to northeast, along the continental margin. We divided these submarine canyons into four different types, Types A, B, C and D, based on their size and morphology (Fig. 3b). Types A, B and

C show a predominant NW-SE orientation, while Type D canyons strike to the north (Fig. 2).

Type A canyons occur in the southwestern part of the study area (Figs. 3b and 7a), and consist of 10 discrete canyons named A1 to A10 (Fig. 7b). They are 10 to 15 km long and 2-4 km wide. The depth of incision of Type A canyons varies from 40 to 120 m (Fig. 7b). The slope gradients of the canyon walls range from 2.4° to 8° (Fig. 7b). Type A canyons lack well-developed canyon heads and few small-scale gullies are observed perpendicularly to the shelf edge (Figs. 7a and 7b).

Type B canyons are located to the northeast of Type A canyons and comprise 10 canyons named B1 to B10 (Fig. 8b). Type B canyons are 15-20 km long and 2.5-7.5 km wide. The incisional depth of Type B canyons ranges from 120 to 240 m (Fig. 8b). The slope gradients of the canyon walls range from 4.8° to 8.4° (Fig. 8b). The heads of Type B canyon are characterised by their well-developed amphitheater rims eroded by submarine gullies (Fig. 8a).

Type C canyons occur in the middle and northeastern parts of the continental margin and consist of 24 distinct canyons (Fig. 3b). They are 15 to 30 km long and 5 to 10 km wide. The depth of incision of Type C canyons varies from 150 to 450 m (Fig. 9b). The slope gradients of the canyon walls range from 8.5° to 14.8° (Fig. 9b). The heads of Type C canyons are characterised by their well-developed amphitheater rims, which are incised by more submarine gullies than in the Type B canyons (Fig. 9a).

Four Type D canyons (D1 to D4) occur in the northeast of the study area (Fig. 3b). Canyon D1 strikes to the NNW and D2-D4 are N-striking features (Fig. 10a). They are relatively narrow (1.5-2 km wide) in their upper parts and become gradually wider (4-5 km) downslope (Fig. 10a). Their lengths range from 45 km to 60 km and their depth of incision ranges from 170 to 580 m (Figs. 10a, 10b, 10c and 10d). The slope gradients of the canyon walls range from 4.5° to 24° (Figs. 10b, 10c and 10d). The heads of Type D canyons show elongated head scarps, not the amphitheater-shaped canyon heads of Types A, B and C (Figs. 7a, 8a, 9a and 10a).

4.3 Internal seismic character of submarine canyons

Seismic profiles parallel to the continental slope in Type A and B canyons show U-shaped, non-continuous seismic reflections (Figs. 11a and 11b). Thalweg incision is observed in shallow strata of Type B canyons (Figs. 11a and 11b). Type C canyons reveal U-shaped, non-continuous seismic reflections between the horizons T40 (10.5 Ma) and T20 (1.9 Ma) (Figs. 12b and 12c). These buried submarine canyons are revealed as migrating to the NE in seismic data (Fig. 12b). In addition, buried canyons are filled by chaotic to poorly continuous strata (Figs. 12b and 12c). Blind faults can also be observed close to Type C canyons on the shelf margin, which has been tectonically active before the Late Miocene (Fig. 12a). The erosional surface of Type D canyons shows U-shaped seismic reflections above horizon T40 (10.5 Ma) (Figs. 13a and 13b). Relatively high-amplitude reflections with low continuity occur close to these erosional features (canyons), and are interpreted as basal lag deposits (Fig. 13b). Recurrent MTDs, showing chaotic reflections with low amplitude to transparent seismic facies, are interpreted above the interpreted basal lags (Fig. 13b). Lateral accretion packages occur near the western flanks of canyons and are characterised by their moderate-amplitude internal reflections (Fig. 13b). The MTDs previously described occur in the center of canyons (Fig. 13b).

A U-shaped, down-cutting reflector is observed in the Central Canyon between horizons T30 and T40 (Fig. 6c). Seismic profiles show discontinuous high-amplitude reflections on the continental shelf above horizon T30, and coeval chaotic reflections on the continental slope (Figs. 6a and 6c).

5 Discussion

5.1 Origin and evolution of submarine canyons on the northwest South China Sea margin

The most common phenomena that result in the development of submarine canyons are: 1) slumping, retrogressive slope failures and other mass-wasting events (Farre et al., 1983; Pratson and Coakley, 1996); 2) the downslope flow of erosive turbidity currents sourced from fluvial, shelf and upper continental slope areas (Shepard, 1981; Pratson et al., 1994; Harris and Whiteway, 2011); 3) the cascading of sediment-laden subglacial meltwater in glaciated margins (Gales et al., 2021). Retrogressive slope failure usually occurs on the upper continental slope to eventually form broad amphitheater-shaped heads at the shelf edge (Farre et al., 1983; Pratson and Coakley, 1996). Slope failures can ultimately lead to the formation of a shelf-indenting canyon regardless if it is linked, or not, to the mouth of a river on the continental shelf (Pratson and Coakley, 1996).

In the study area, 48 submarine canyons were formed at a water depth ranging from 200-2000 m (Fig. 3). These submarine canyons are shelf-incised canyons (Fig. 3a), and bathymetric data show semicircular or elliptic depressions in the heads of Type A to C canyons that likely resulted from the early generation of arcuate slide scars (Figs. 7a, 8a and 9a). Chaotic reflections indicate the presence of recurrent mass-transport deposits (MTDs) in the uppermost part of these submarine canyons (Fig. 12c), suggesting they were formed by the retrogressive slope failure of the canyon heads. When the upper slope gradient exceeds its equilibrium grade, erosion ensues via the slumping and overall gravitational collapse of the slope, and sediment bypasses the shelf on its way to the lower continental slope (Ross et al., 1994; Xie et al., 2008). Moreover, retrogressive slope failure in the study area could have been associated to turbidity currents, thus enhancing the more common slope-eroding processes (Pratson and Coakley, 1996; Green et al., 2007; Harris and Whiteway, 2011). Multiple dendritic submarine gullies can be observed in the canyon heads, thus suggesting that successive sediment flows deepened and widened Types A to C submarine canyons by recurrent seafloor erosion (Figs. 3a, 7a and 8a and 9a).

The northeastern margin of the Qiongdongnan Basin began to form at the start of the Late

Miocene (~10.5 Ma; Xie et al., 2008; Yin et al., 2011). Recurrent slumping and gravity flows occurred frequently due to local tectonic movement in the northeastern sector of the Qiongdongnan Basin (Chen et al., 1993; Xie et al., 2008; Chen et al., 2016). The basal erosional surfaces of Type C and D canyons reveal they started forming at the Late Miocene (Figs. 12 and 13). In addition, the U-shaped high-amplitude reflections represent the basal erosional surfaces of several Type A and B submarine canyons, thus suggesting that these canyons were also formed after the Quaternary (1.9 Ma) (Figs. 6a, 6b, 11a and 11b).

5.2 Controls on canyon morphology along the northwest South China Sea margin

Submarine canyon morphology is affected by multiple controlling factors, including sediment supply (Harris and Whiteway, 2011), regional tectonic events (Dantec et al., 2010; Moutjoy et al., 2018), contour currents (Liu et al., 2019; Miramontes et al., 2020), internal waves (Kunze et al., 2002), or a combination of all these phenomena. The bathymetric data interpreted in this work show that canyon morphology varies along the northwest South China Sea continental margin. The number of canyons, the scale of canyons, and the gradient of canyon walls all increase from southwest to northeast (Figs. 3, 7, 8, 9 and 10).

In the study area, sediment in the northwest South China Sea margin is mostly derived from three areas: the Red River, the Pearl River and Hainan Island (Chen et al., 2016; Zhao et al., 2019; Chen et al., 2020). Sediment derived from the Red River (~10 Mt/yr) can be transported to four types of submarine canyons via the action of continental-shelf currents (Liu et al., 2015; Zhao et al., 2019; Fig. 2). Type A and B canyons receive more sediment than Type C and D canyons because they are closer to the Red River (Zhao et al., 2019; Chen et al., 2020). Due to its longer distance, the Pearl

River transports less volumes than Red River to the study area (Fig. 1). Sediment from the Pearl River can be transported to submarine canyons in this study when surface currents (northeast monsoon and Western Pacific surface water) in winter are relatively stronger (Liu et al., 2014). Sediment discharge from Hainan Island only totals 0.6 Mt/yr (Zhao et al., 2019), thus justifying why sediment transport to Type A and B canyons is larger in volume than that in Types C and D canyons.

Shelf-margin architecture in the southwest Qiongdongnan Basin reveals a progradational trend, and an aggradational pattern in its northeast, suggesting high sedimentation rates feeding Type A and B canyons (Figs. 6a and 6b). When sediment accumulation exceeds local accommodation space on the continental slope, and submarine canyons' capacity to transport sediment downslope, they become filled or even buried (Saller and Dharmasamadhi 2012; Puig et al., 2017). This is consistent with the Type A and B canyons interpreted in this work (Figs. 7a and 8a).

Tectonic events also play a significant role in the development of submarine canyons (Mountjoy et al., 2009; Micallef et al., 2014). Key examples are the submarine canyons of the northern slope of the Little Bahama Bank (Mulder et al., 2012). Submarine canyons located in the eastern part of the Bahamas slope are longer, deeper, wider, more incised, and present a lower sinuosity than those in the western part (Mulder et al., 2012; 2018). Such a character has been justified by tectonic tilting of the Little Bahama Bank (Mulder et al., 2012). Additionally, the tectonic ridges in Moresby Trough are able to trap and redirect sediment, leading to a longer and wider submarine canyon in Gulf of Papua (Francis et al., 2008). In Nankai, SE Japan, submarine gullies are also known to vary in their incision depth relative to the activity of underlying thrust faults, i.e., the larger the uplift associated with thrust-fault activity the deeper submarine gullies incise the continental slope off Nankai (Alves et al, 2014).

In this study, a large-scale ENE-trending normal fault (No.2 fault) is located to the north of the

48 submarine canyons investigated in the Qiongdongnan Basin (Fig. 1; Xie et al., 2008; Hu et al., 2013). It comprises a seaward-dipping fault system leading to the development of a relatively steep continental slope (Zhuo et al., 2018). The long-term activity of the No.2 fault created a sediment-starved zone off the continental shelf in Type C and D canyons that was hard for sediment to fill and for progradation to take place; consequently, sediments accumulated on the continental shelf reveal an aggradation trend (Fig. 6c). This led to local oversteepening in Type C and D canyons, promoting the occurrence of slumps or slides (Figs. 6c and 12c). Sediment flows induced by oversteepening and localised slope failure are considered the major drivers of canyon initiation (Micallef et al., 2014), correlating with the presence of gullies in the canyon heads in Type C canyons (Fig. 9).

5.3 Implications for the evolution of a giant submarine canyon system

This study reveals the importance of submarine canyons as sources of sediment to large-scale submarine conduits or canyon systems formed at the base of the continental slope (Figs. 1 and 2). The Central Canyon system is located to the south of the 48 submarine canyons studied here, and presents a clear E-W orientation (Figs. 1 and 2). It was generated at the end of the Miocene (5.5 Ma) and its western and central parts were rapidly buried (Yuan et al., 2009; Gong et al., 2011; Li et al., 2013; Su et al., 2014). Recurrent mass-transport deposits (MTDs) are observed in the Central Canyon System above horizon T30 (5.5 Ma) in its western and middle segments. These MTDs were sourced from the southwestern and middle parts of the Qiongdongnan Basin (Figs. 6a and 6c; Gong et al., 2011; Su et al., 2014).

Type A and B canyons feed into the western part of the Central Canyon system (Fig. 2). In the Late Miocene (after 5.5 Ma), the Red River provided vast amounts of sediment to the Qiongdongnan

Basin in response to rapid tectonic uplift of the Tibetan Plateau (Chen et al., 2016; Zhao et al., 2019). High sediment supply and sedimentation rates likely resulted in poor cementation of sediment in Type A and B canyons, i.e., decreasing the shear strength of seafloor sediment and promoting more frequent slope instability. Type C and D canyons are observed near the mid part of the Central Canyon system (Figs. 2 and 3). Since the Early Pliocene, reactivation of regional extensional faults (e.g. No. 12 fault) in Type C and D canyons has triggered slope instability and caused multiple submarine landslides (Xie et al., 2006; He et al., 2013; Sun et al., 2015). Recurrent MTDs sourced from the upper slope were delivered downslope and trapped by the Central Canyon system. These MTDs led to the gradual infill of the middle part of the Central Canyon system.

On the Little Bahamas Bank, a giant submarine canyon (the Great Abaco Canyon) with a length of 135 km and a NW-SE orientation was fed by sediment supplied from the Bank itself, maintaining its structure and morphology (Mulder et al., 2018). In contrast to the Great Abaco Canyon, this study proves that submarine canyons can accelerate the infilling process of an adjacent, large-scale submarine canyon instead of only promoting, or maintaining, its development.

Canyon-fill deposits comprising sandy intervals can host large hydrocarbon reservoirs (Posamentier and Kolla, 2003; Wu et al., 2009). In the study area, two gas fields (LS22-1 and LS17-2) occur in the western part of the Central Canyon at a water depth over 1300 m, with an estimated volume of gas in place of more than 1132×10^8 m^3 (Huang et al., 2016). Gas hydrates are also present in the GMGS5 drilling area, which is located in the middle reach of the Central Canyon system at a water depth ranging from 1600 m to 1800 m (Liang et al., 2019; Wei et al., 2019). The sediment filling the western part of the Central Canyon system is composed of coarse-grained turbidites and sheet sand-MTDs (Su et al., 2014). The middle reach of Central Canyon is filled by sand sheets and large-scale MTDs sourced from the northern margin (Shang et al., 2015). This indicates that the west and middle reaches of the Central Canyon system may comprise good hydrocarbon reservoirs.

6 Conclusions

In this paper we describe, for the first time, the detailed geomorphology, origin and evolution of submarine canyons along the northwest South China Sea margin based on high-resolution bathymetric and 2D seismic data. The main conclusions of this study are as follows.

(1) We identify 48 submarine canyons on the northwest South China Sea margin, which can be classified as shelf-incised submarine canyons. These submarine canyons are divided into four different types (Types A, B, C and D) based on their morphology and sizes.

(2) Type A lacks well-developed canyon heads, being 10-15 km long and 2-4 km wide. Type B canyons are 15-20 km long and 2.5-7.5 km wide. Type B canyon heads show well-developed amphitheater rims, which were eroded by several gullies. The length of Type C canyons ranges from 15 to 30 km, whereas their width varied from 5 to 10 km. Type C canyon heads are also characterized by well-developed amphitheater rims, and reveal more gullies than Type B. Type D canyons are N-S oriented and are 45-60 km long. They are relatively narrow (1.5-2 km wide) in their upper parts but broaden (4-5 km) in their lower reaches.

(3) We infer that the investigated submarine canyons were generated by retrogressive slope failure at the start of the Late Miocene (10.5 Ma). We conclude that recurrent MTDs caused by submarine failure accelerate the filling of the western and middle reaches of Central Canyon system. The sediment filling the Central Canyon system may play a significant role in accumulating oil and gas in this latter region.

Acknowledgments

We acknowledge China National Offshore Oil Corporation for their permissions to release the seismic data in this work. This research was financially supported by Key Special Project for Introduced Talents Team of Southern Marine Science and Engineering Guangdong Laboratory (Guangzhou) (GML2019ZD0104), Guangdong Basic and Applied Basic Research Foundation (2020B1515020016), National Natural Science Foundation of Guangdong Province (2020A1515010497), National Scientific Foundation of China (41876054) and Guangdong Pearl River Talents Program (2017GC010510). We gratefully acknowledge the advices and constructive comments from Dr. Rui Quartau and Dr. Yunlong He. Dr. Wei Li is specially funded by CAS Pioneer Hundred Talents Program.

References

Alves, T.M., Moore, G.F., Strasser, M., 2014. Erosional features as indicators of thrust fault activity (Nankai Trough, Japan). Marine Geology 356, 5-18.

Baztan, J., Berné, S., Olivet, J.-L., Rabineau, M., Aslanian, D., Gaudin, M., Réhault, J.-P., Canals, M., 2005. Axial incision: The key to understand submarine canyon evolution (in the western Gulf of Lion). Marine Petroleum Geology 22, 805-826.

Canals, M., Puig, P., de Madron, X.D., Heussner, S., Palanques, A., Fabres, J., 2006. Flushing submarine canyons. Nature 444, 354-357.

Carvajal, C., Steel, R., Petter, A., 2009. Sediment supply: The main driver of shelf-margin growth. Earth-Science Reviews 96, 221-248.

Chen, H., Zhan, W., Wu, S., 2016. Response of geomorphic and geological processes to insufficient and ample sediment supply along the upper continental slope in the north-western South China Sea. Journal of Earth

System Science 125, 1635-1655.

Chen, P.P., Chen, Z.Y., Zhang, Q.M., 1993. Sequence stratigraphy and continental margin development of the northwestern shelf of the South China Sea. AAPG bulletin 77, 842-862.

Chen, S., Steel, R., Wang, H., Zhao, R., Olariu, C., 2020. Clinoform growth and sediment flux into late Cenozoic Qiongdongnan shelf margin, South China Sea. Basin Research 32, 302-319.

Clift, P.D., Sun, Z., 2006. The sedimentary and tectonic evolution of the Yinggehai–Song Hong basin and the southern Hainan margin, South China Sea: Implications for Tibetan uplift and monsoon intensification. Journal of Geophysical Research: Solid Earth 111.

Covault, J.A., Normark, W.R., Romans, B.W., Graham, S.A., 2007. Highstand fans in the California borderland: The overlooked deep-water depositional systems. Geology 35, 783-786.

Curray, J.R., Emmel, F.J., Moore, D.G., 2002. The Bengal Fan: morphology, geometry, stratigraphy, history and processes. Marine and Petroleum Geology, 19, 1191-1223.

de Stigter, H.C., Jesus, C.C., Boer, W., Richter, T.O., Costa, A., van Weering, T.C., 2011. Recent sediment transport and deposition in the Lisbon–Setúbal and Cascais submarine canyons, Portuguese continental margin. Deep Sea Research Part II: Topical Studies in Oceanography 58, 2321-2344.

Ding, W., Li, J., Han, X., Suess, E., Huang, Y., Qiu, X., Li, M., 2010. Morphotectonics and formation of the Taiwan Bank Canyon, southwest offshore Taiwan Island. Journal of Oceanography and Marine Science 1, 65-78.

Ding, W., Li, J., Li, J., Fang, Y., Tang, Y., 2013. Morphotectonics and evolutionary controls on the Pearl River canyon system, South China Sea. Marine Geophysical Research 34, 221-238.

Farre, J.A., McGregor, B.A., Ryan, W.B., Robb, J.M., 1983. Breaching the shelfbreak: passage from youthful to mature phase in submarine canyon evolution. AAPG bulletin.

Francis, J.M., Daniell, J.J., Droxler, A.W., Dickens, G.R., Bentley, S.J., Peterson, L.C., Opdyke, B.N., Beaufort, L., 2008. Deep water geomorphology of the mixed siliciclastic-carbonate system, Gulf of Papua. Journal of

Geophysical Research: Earth Surface 113.
Gales, J., Rebesco, M., De Santis, L., Bergamasco, A., Colleoni, F., Kim, S., Accettella, D., Kovacevic, V., Liu, Y., Olivo, E., Colizza, E., Florindo-Lopez, C., Zgur, F., McKay, R., 2021. Role of dense shelf water in the development of Antarctic submarine canyon morphology. Geomorphology, 372, art. no. 107453
Gingele, F.X., De Deckker, P., Hillenbrand, C.-D., 2004. Late Quaternary terrigenous sediments from the Murray Canyons area, offshore South Australia and their implications for sea level change, palaeoclimate and palaeodrainage of the Murray–Darling Basin. Marine Geology 212, 183-197.
Goff, J.A., 2001. Quantitative classification of canyon systems on continental slopes and a possible relationship to slope curvature. Geophysical Research Letters 28, 4359-4362.
Gong, C., Wang, Y., Rebesco, M., Salon, S., Steel, R.J., 2018. How do turbidity flows interact with contour currents in unidirectionally migrating deep-water channels? Geology, 46 (6), pp. 551-554.
Gong, C., Wang, Y., Zhu, W., Li, W., Xu, Q., 2013. Upper Miocene to Quaternary unidirectionally migrating deep-water channels in the Pearl River Mouth Basin, northern South China Sea. AAPG bulletin 97, 285-308.
Gong, C., Wang, Y., Zhu, W., Li, W., Xu, Q., Zhang, J., 2011. The central Submarine Canyon in the Qiongdongnan Basin, northwestern South China Sea: Architecture, sequence stratigraphy, and depositional processes. Marine Petroleum Geology 28, 1690-1702.
Green, A.N., Goff, J.A., Uken, R., 2007. Geomorphological evidence for upslope canyon-forming processes on the northern KwaZulu-Natal shelf, SW Indian Ocean, South Africa. Geo-Marine Letters 27, 399-409.
Harris, P.T., Whiteway, T., 2011. Global distribution of large submarine canyons: Geomorphic differences between active and passive continental margins. Marine Geology 285, 69-86.
He, Y., Xie, X., Kneller, B.C., Wang, Z., Li, X., 2013. Architecture and controlling factors of canyon fills on the shelf margin in the Qiongdongnan Basin, northern South China Sea. Marine Petroleum Geology 41, 264-276.
Hu, B., Wang, L., Yan, W., Liu, S., Cai, D., Zhang, G., Zhong, K., Pei, J., Sun, B., 2013. The tectonic evolution of

the Qiongdongnan Basin in the northern margin of the South China Sea. Journal of Asian Earth Sciences 77, 163-182.
Huang, B., Tian, H., Li, X., Wang, Z., Xiao, X., 2016. Geochemistry, origin and accumulation of natural gases in the deepwater area of the Qiongdongnan Basin, South China Sea. Marine Petroleum Geology 72, 254-267.
Iacono, C.L., Sulli, A., Agate, M., 2014. Submarine canyons of north-western Sicily (Southern Tyrrhenian Sea): Variability in morphology, sedimentary processes and evolution on a tectonically active margin. Deep Sea Research Part II: Topical Studies in Oceanography 104, 93-105.
Iacono, C.L., Sulli, A., Agate, M., Presti, V.L., Pepe, F., Catalano, R., 2011. Submarine canyon morphologies in the Gulf of Palermo (Southern Tyrrhenian Sea) and possible implications for geo-hazard. Marine Geophysical Research 32, 127-138.
Jobe, Z.R., Lowe, D.R., Uchytil, S.J., 2011. Two fundamentally different types of submarine canyons along the continental margin of Equatorial Guinea. Marine Petroleum Geology 28, 843-860.
Krastel, S., Wefer, G., Hanebuth, T.J., Antobreh, A.A., Freudenthal, T., Preu, B., Schwenk, T., Strasser, M., Violante, R., Winkelmann, D., 2011. Sediment dynamics and geohazards off Uruguay and the de la Plata River region (northern Argentina and Uruguay). Geo-Marine Letters 31, 271-283.
Kunze, E., Rosenfeld, L.K., Carter, G.S., Gregg, M.C., 2002. Internal waves in Monterey submarine canyon. Journal of physical oceanography 32, 1890-1913.
Lastras, G., Arzola, R., Masson, D., Wynn, R., Huvenne, V., Hühnerbach, V., Canals, M., 2009. Geomorphology and sedimentary features in the Central Portuguese submarine canyons, Western Iberian margin. Geomorphology 103, 310-329.
Le Dantec, N., Hogarth, L.J., Driscoll, N.W., Babcock, J.M., Barnhardt, W.A., Schwab, W.C., 2010. Tectonic controls on nearshore sediment accumulation and submarine canyon morphology offshore La Jolla, Southern California. Marine Geology 268, 115-128.

Li, C.F., Xu, X., Lin, J., Sun, Z., Zhu, J., Yao, Y., Zhao, X., Liu, Q., Kulhanek, D.K., Wang, J., 2014. Ages and magnetic structures of the South China Sea constrained by deep tow magnetic surveys and IODP Expedition 349. Geochemistry, Geophysics, Geosystems 15, 4958-4983.

Li, W., Alves, T.M., Wu, S., Völker, D., Zhao, F., Mi, L., Kopf, A., 2015. Recurrent slope failure and submarine channel incision as key factors controlling reservoir potential in the South China Sea (Qiongdongnan Basin, South Hainan Island). Marine Petroleum Geology 64, 17-30.

Li, X.Q, Fairweather, L., Wu, S., Ren, J., Zhang, H., Quan, X., Jiang, T., Zhang, C., Su, M., He, Y., 2013. Morphology, sedimentary features and evolution of a large palaeo submarine canyon in Qiongdongnan basin, Northern South China Sea. Journal of Asian Earth Sciences 62, 685-696.

Li, C., Lv, C., Chen, G., Zhang, G., Ma, M., Shen, H., Zhao, Z., Guo, S., 2017. Source and sink characteristics of the continental slope-parallel Central Canyon in the Qiongdongnan Basin on the northern margin of the South China Sea. Journal of Asian Earth Sciences 134, 1-12.

Liang, C., Liu, C., Xie, X., Yu, X., He, Y., Chen, H., Zhou, Z., Tian, D., Lu, B., Mi, H., 2020. The role of large-scale mass wasting processes in changing the sediment dispersal pattern in the deep-water Central Canyon of the northwestern South China Sea. Marine Petroleum Geology 122, 104693.

Liu, J.G., Clift, P.D., Yan, W., Chen, Z., Chen, H., Xiang, R., Wang D.X., 2014. Modern transport and deposition of settling particles in the northern South China Sea: sediment trap evidence adjacent to Xisha Trough. Deep Sea Research Part I: Oceanographic Research Papers 93, 145-155.

Liu, S., Van Rooij, D., Vandorpe, T., González-Pola, C., Ercilla, G., Hernández-Molina, F.J., 2019. Morphological features and associated bottom-current dynamics in the Le Danois Bank region (southern Bay of Biscay, NE Atlantic): A model in a topographically constrained small basin. Deep Sea Research Part I: Oceanographic Research Papers 149, 103054.

Ma, B., Wu, S., Sun, Q., Mi, L., Wang, Z., Tian, J., 2015. The late Cenozoic deep-water channel system in the

Baiyun Sag, Pearl River Mouth Basin: Development and tectonic effects. Deep Sea Research Part II: Topical Studies in Oceanography 122, 226-239.

Mansurbeg, H., De Ros, L., Morad, S., Ketzer, J., El-Ghali, M., Caja, M., Othman, R., 2012. Meteoric-water diagenesis in late Cretaceous canyon-fill turbidite reservoirs from the Espírito Santo Basin, eastern Brazil. Marine Petroleum Geology 37, 7-26.

Micallef, A., Mountjoy, J.J., Barnes, P.M., Canals, M., Lastras, G., 2014. Geomorphic response of submarine canyons to tectonic activity: Insights from the Cook Strait canyon system, New Zealand. Geosphere 10, 905-929.

Miramontes, E., Eggenhuisen, J.T., Jacinto, R.S., Poneti, G., Pohl, F., Normandeau, A., Campbell, D.C., Hernández-Molina, F.J., 2020. Channel-levee evolution in combined contour current–turbidity current flows from flume-tank experiments. Geology 48, 353-357.

Mountjoy, J.J., Howarth, J.D., Orpin, A.R., Barnes, P.M., Bowden, D.A., Rowden, A.A., Schimel, A.C., Holden, C., Horgan, H.J., Nodder, S.D., 2018. Earthquakes drive large-scale submarine canyon development and sediment supply to deep-ocean basins. Science advances 4, eaar3748.

Mulder, T., Joumes, M., Hanquiez, V., Gillet, H., Reijmer, J., Tournadour, E., Chabaud, L., Principaud, M., Schnyder, J., Borgomano, J., 2017. Carbonate slope morphology revealing sediment transfer from bank-to-slope (Little Bahama Bank, Bahamas). Marine Petroleum Geology 83, 26-34.

Mulder, T., Zaragosi, S., Garlan, T., Mavel, J., Cremer, M., Sottolichio, A., Sénéchal, N., Schmidt, S., 2012. Present deep-submarine canyons activity in the Bay of Biscay (NE Atlantic). Marine Geology 295, 113-127.

Pratson, L.F., Coakley, B.J., 1996. A model for the headward erosion of submarine canyons induced by downslope-eroding sediment flows. Geological Society of America Bulletin 108, 225-234.

Pratson, L.F., Ryan, W.B., Mountain, G.S., Twichell, D.C., 1994. Submarine canyon initiation by downslope-eroding sediment flows: evidence in late Cenozoic strata on the New Jersey continental slope. Geological

Society of America Bulletin 106, 395-412.

Puig, P., Durán, R., Muñoz, A., Elvira, E., Guillén, J., 2017. Submarine canyon-head morphologies and inferred sediment transport processes in the Alías-Almanzora canyon system (SW Mediterranean): On the role of the sediment supply. Marine Geology 393, 21-34.

Puig, P., Ogston, A., Mullenbach, B., Nittrouer, C., Sternberg, R., 2003. Shelf-to-canyon sediment-transport processes on the Eel continental margin (northern California). Marine Geology 193, 129-149.

Qiao, S., Su, M., Kuang, Z., Yang, R., Liang, J., Wu, N., 2015. Canyon-related undulation structures in the Shenhu area, northern South China Sea. Marine Geophysical Research 36, 243-252.

Ren, J., Wang, H., Sun, M., Gan, H., Song, G., Sun, Z., 2014. Sequence stratigraphy and sedimentary facies of Lower Oligocene Yacheng Formation in deepwater area of Qiongdongnan Basin, Northern South China Sea: Implications for coal-bearing source rocks. Journal of Earth Science 25, 871-883.

Ross, W., Halliwell, B., May, J., Watts, D., Syvitski, J., 1994. Slope readjustment: a new model for the development of submarine fans and aprons. Geology 22, 511-514.

Saller, A., Dharmasamadhi, I.N.W., 2012. Controls on the development of valleys, canyons, and unconfined channel–levee complexes on the Pleistocene Slope of East Kalimantan, Indonesia. Marine Petroleum Geology 29, 15-34.

Shang, Z., Xie, X., Li, X., Zhang, D., He, Y., Yang, X., Cui, M., 2015. Difference in full-filled time and its controlling factors in the central canyon of the Qiongdongnan Basin. Acta Oceanologica Sinica 34, 81-89.

Shao, L., Cui, Y., Stattegger, K., Zhu, W., Qiao, P., Zhao, Z., 2019. Drainage control of Eocene to Miocene sedimentary records in the southeastern margin of Eurasian Plate. Geological Society of America Bulletin 131, 461-478.

Shepard, F.P., 1981. Submarine canyons: multiple causes and long-time persistence. AAPG bulletin 65, 1062-1077.

Shi, W., Xie, Y., Wang, Z., Li, X., Tong, C., 2013. Characteristics of overpressure distribution and its implication for hydrocarbon exploration in the Qiongdongnan Basin. Journal of Earth Science 66, 150-165.

Su, M., Xie, X., Xie, Y., Wang, Z., Zhang, C., Jiang, T., He, Y., 2014. The segmentations and the significances of the Central Canyon System in the Qiongdongnan Basin, northern South China Sea. Journal of Asian Earth Sciences 79, 552-563.

Su, M., Lin, Z., Wang, C., Kuang, Z., Liang, J., Chen, H., Liu, S., Zhang, B., Luo, K., Huang, S., 2020. Geomorphologic and infilling characteristics of the slope-confined submarine canyons in the Pearl River Mouth Basin, northern South China Sea. Marine Geology 424, 106166.

Sun, Z., Wang, Z., Sun, Z., Wang, Z., Zhang, W., He, L., 2015. Structure and kinematic analysis of the deepwater area of the Qiongdongnan Basin through a seismic interpretation and analogue modeling experiments. Acta Oceanologica Sinica 34, 32-40.

Taylor, B., Hayes, D.E., 1983. Origin and history of the South China Sea basin. The tectonic geologic evolution of Southeast Asian seas islands: Part 2 27, 23-56.

Tournadour, E., Mulder, T., Borgomano, J., Gillet, H., Chabaud, L., Ducassou, E., Hanquiez, V., Etienne, S., 2017. Submarine canyon morphologies and evolution in modern carbonate settings: The northern slope of Little Bahama Bank, Bahamas. Marine Geology 391, 76-97.

Wang, L., Wu, S.-G., Li, Q.-P., Wang, D.-W., Fu, S.-Y., 2014. Architecture and development of a multi-stage Baiyun submarine slide complex in the Pearl River Canyon, northern South China Sea. Geo-Marine Letters 34, 327-343. Wei, J., Liang, J., Lu, J., Zhang, W., He, Y., 2019. Characteristics and dynamics of gas hydrate systems in the northwestern South China Sea-Results of the fifth gas hydrate drilling expedition. Marine Petroleum Geology 110, 287-298.

Wilber, R.J., Milliman, J.D., Halley, R.B., 1990. Accumulation of bank-top sediment on the western slope of Great Bahama Bank: rapid progradation of a carbonate megabank. Geology 18, 970-974.

Wu, S., Yuan, S., Zhang, G., Ma, Y., Mi, L., Xu, N., 2009. Seismic characteristics of a reef carbonate reservoir and implications for hydrocarbon exploration in deepwater of the Qiongdongnan Basin, northern South China Sea. Marine Petroleum Geology 26, 817-823.

Wu, S., Yang, Z., Wang, D., Lü, F., Lüdmann, T., Fulthorpe, C., Wang, B., 2014. Architecture, development and geological control of the Xisha carbonate platforms, northwestern South China Sea. Marine Geology 350, 71-83.

Xie, X., Müller, R.D., Li, S., Gong, Z., Steinberger, B., 2006. Origin of anomalous subsidence along the Northern South China Sea margin and its relationship to dynamic topography. Marine Petroleum Geology 23, 745-765.

Xie, X., Müller, R.D., Ren, J., Jiang, T., Zhang, C., 2008. Stratigraphic architecture and evolution of the continental slope system in offshore Hainan, northern South China Sea. Marine Geology 247, 129-144.

Xu, S., Wang, Y., Peng, X., Zou, H., Qiu, Y., Gong, C., Zhuo, H., 2014. Origin of Taiwan Canyon and its effects on deepwater sediment. Science China Earth Sciences 57, 2769-2780.

Yin, X., Ren, J., Lei, C., Wang, S., Zhang, J., 2011. Postrift rapid subsidence characters in Qiongdongnan Basin, South China Sea. Journal of Earth Science 22, 273-279.

Yuan, S., Lü, F., Wu, S., Yao, G., Ma, Y., Fu, Y., 2009. Seismic stratigraphy of the Qiongdongnan deep sea channel system, northwest South China Sea. Chinese Journal of Oceanology Limnology 27, 250-259.

Zhao, R., Chen, S., Olariu, C., Steel, R., Zhang, J., Wang, H., 2019. A model for oblique accretion on the South China Sea margin; Red River (Song Hong) sediment transport into Qiongdongnan Basin since Upper Miocene. Marine Geology 416, 106001.

Zhao, Z., Sun, Z., Wang, Z., Sun, Z., Liu, J., Zhang, C., 2015. The high resolution sedimentary filling in Qiongdongnan Basin, northern South China Sea. Marine Geology 361, 11-24.

Zhu, M., Graham, S., McHargue, T., 2009a. The red river fault zone in the Yinggehai Basin, South China Sea. Tectonophysics 476, 397-417.

Zhu, M., Graham, S., Pang, X., McHargue, T., 2010. Characteristics of migrating submarine canyons from the middle Miocene to present: implications for paleoceanographic circulation, northern South China Sea. Marine Petroleum Geology 27, 307-319.

Zhu, W.L, Zhong, K, Li, Y.C., Qu, X., Fang, D.Y., 2012. Characteristics of hydrocarbon accumulation and exploration potential of the northern South China Sea deepwater basins. Chinese Science Bulletin 57, 3121-3129.

Zhuo, H., Wang, Y., Sun, Z., Wang, Y., Xu, Q., Hou, P., Wang, X., Zhao, Z., Zhou, W., Xu, S., 2019. Along-strike variability in shelf-margin morphology and accretion pattern: An example from the northern margin of the South China Sea. Basin Research 31, 431-460.

Figure Captions

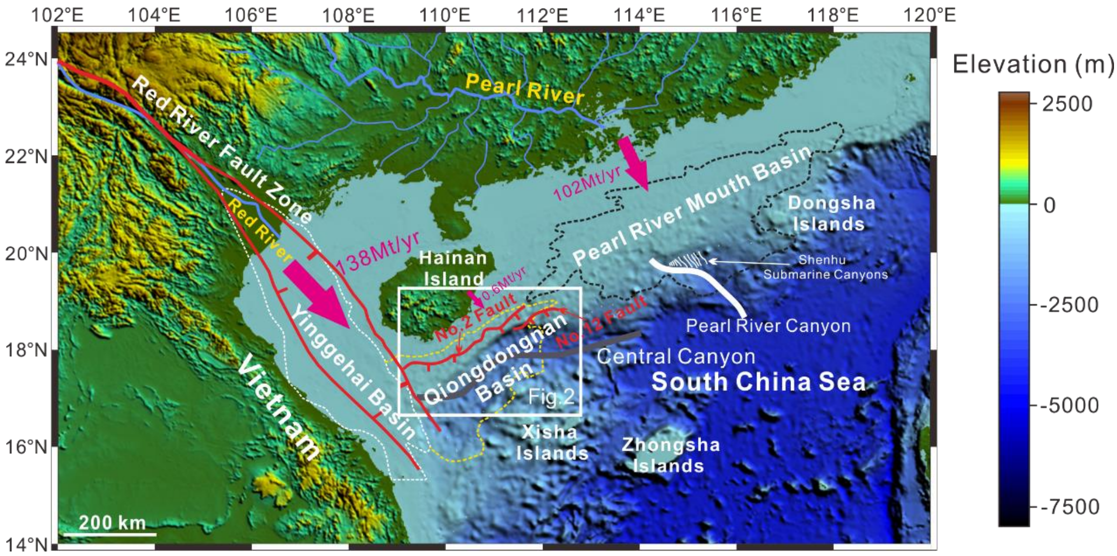

Fig. 1 Regional bathymetric and topographic maps showing the location of major sedimentary basins (e.g. Yinggehai, Pearl River Mouth and Qiongdongnan basins) and geomorphological features (e.g. Dongsha Islands, Zhongsha Islands, Xisha Islands and the Central Canyon) in the northern South China Sea. The boundary of Yinggehai, Pearl River Mouth and Qiongdongnan basin are marked by white, black and yellow dotted lines. The red solid lines indicate the location of Red River Fault Zone, No.2 fault and No.12 fault. The Central Canyon system is highlighted by the grey solid line. The white lines indiacte the location of the Pearl River Canyon and Shenhu submarine canyons. The red box represents the location of Figure 2. The blue lines mark the distribution of Pearl River and Red River. The pink allows indicate the fluvial sediment flux from the Red River, the Pearl River and Hainan Island (modified from Liu et al., 2016 and Zhao et al., 2019). The size of arrows indicates the amount of sediment.

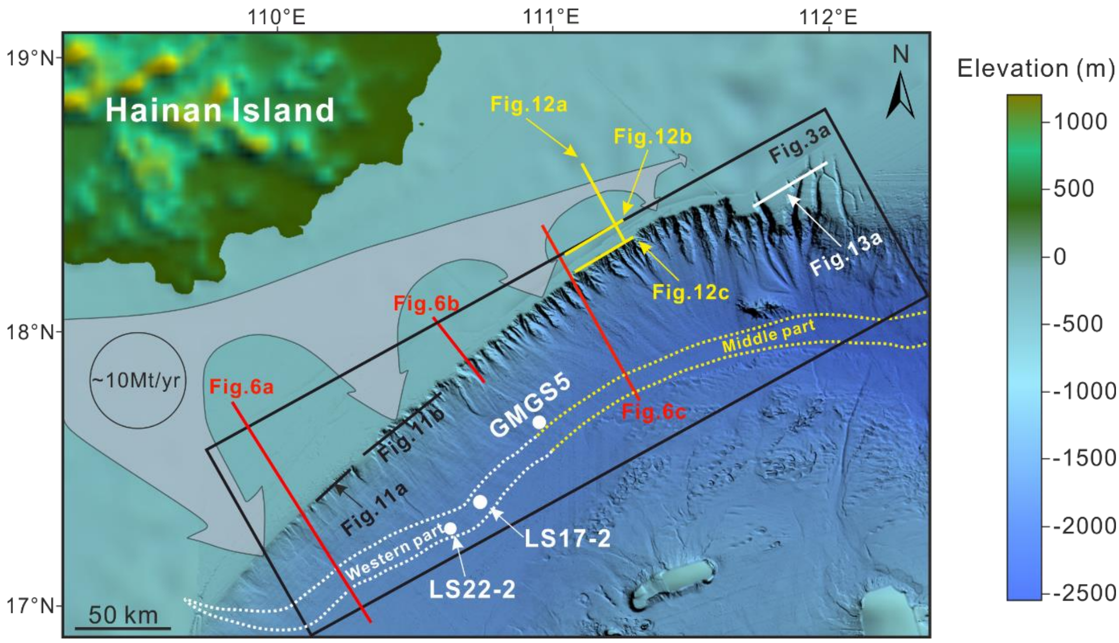

Fig. 2 Multibeam bathymetric map showing the geomorphology of the northwest South China Sea margin and numerous submarine canyons. The black box marks the bathymetric map in Figure 3a. The white and yellow dotted line indicates the canyon rim of the western and middle part of Central Canyon, respectively. The red and yellow lines represent the seismic profiles in Figures 6 and 12. The black and white lines indicate the location of Figure 11 and Figure 13a, respectively. The white dots indicate the gas field (LS22-1 and LS17-2) and gas hydrate drilling zone (GMGS5). The route of sediment from the Red River is marked by grey arrows (modified from Zhao et al., 2019). The size of the grey arrows represents the amount of sediment.

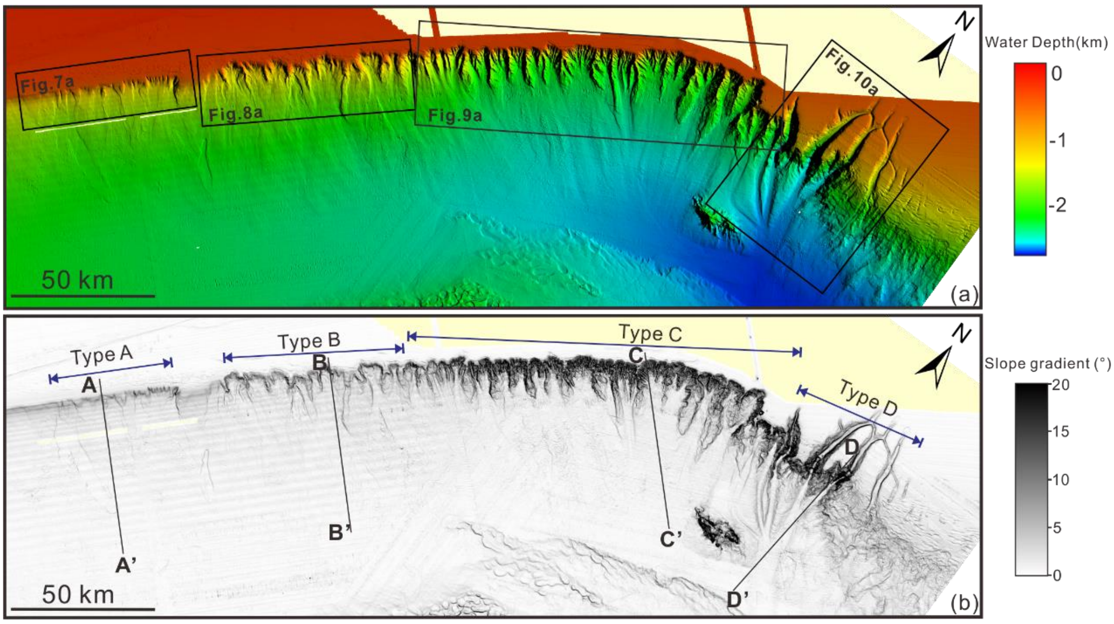

Fig. 3 (a) High-resolution multibeam bathymetric map revealing the detailed morphology of forty-eight (48) shelf-incised submarine canyons (see location in Figure 2). Note that canyon morphology reveals variations from southwest to northeast; submarine canyons are larger and more incised towards the northeast. (b) Slope gradient map of the forty-eight shelf-incised submarine canyons denoting that the gradient of the canyon walls increases from southwest to northeast. The black solid lines highlight the cross-sections shown in Figure 5.

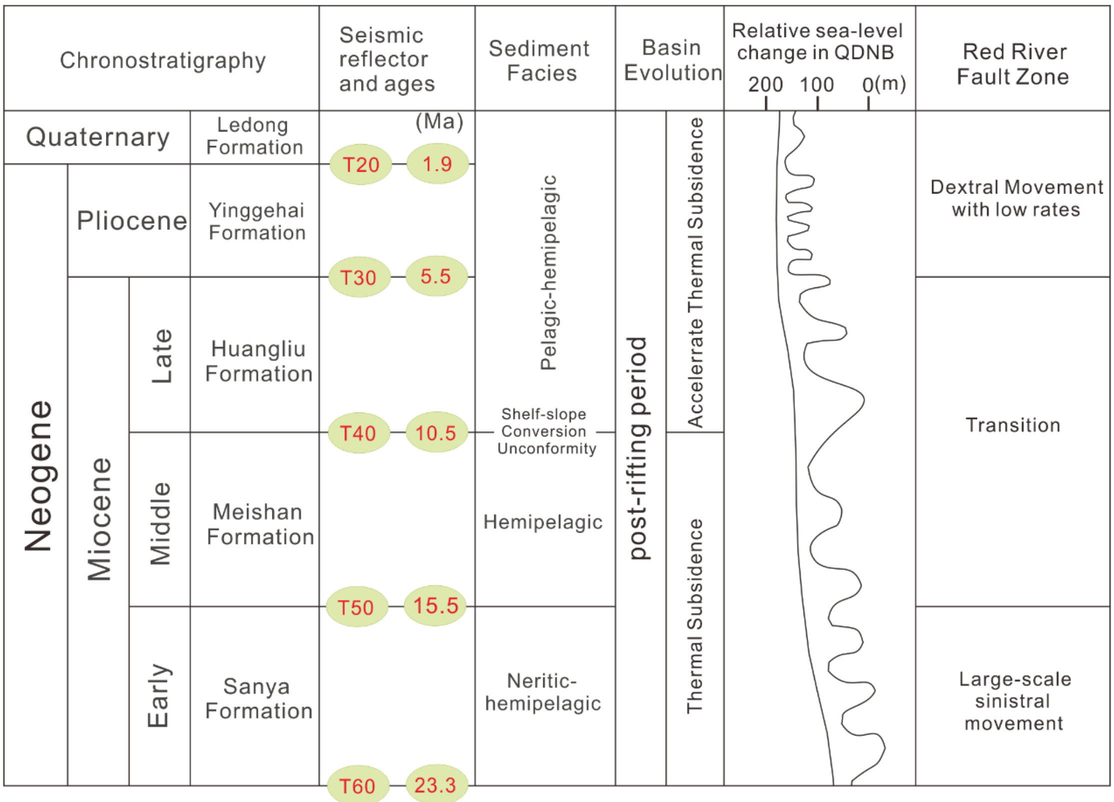

Fig. 4 Schematic stratigraphic panel for the Qiongdongnan Basin. In the panel are shown the chronostratigraphy, main seismic reflectors, sea-level variations, tectonic events and sedimentary environments of the basin (modified after Wang et al., 2014, Li et al., 2013 and Wu et al., 2009). The ages of regional seismic-stratigraphic markers are based on published data from Wang et al. (2014), Wu et al., (2014) and Li et al. (2015). The relative sea-level curve for the Qiongdongnan Basin was taken from Wei et al. (2001).

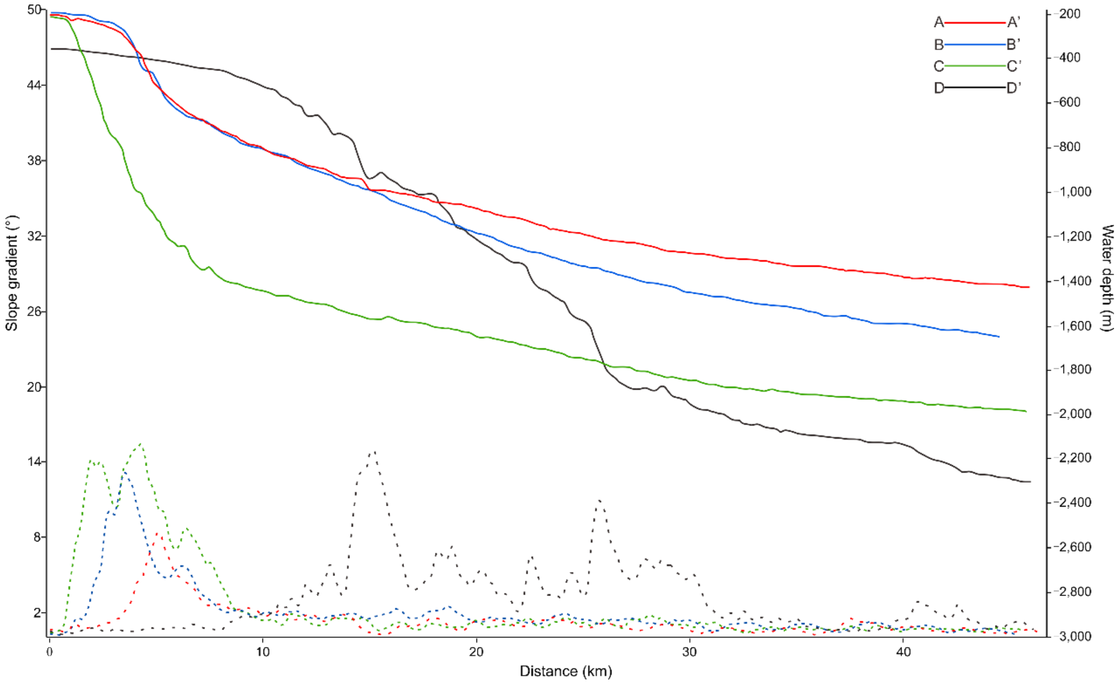

Fig. 5 Bathymetric profiles highlighting the morphology of the continental margin at four different locations in the northwest South China Sea margin (location of profiles is shown in Figure 3b). The dashed lines indicate the variations of slope gradients (filtered by expoentional moving average method) from the continental shelf to the lower continental slope.

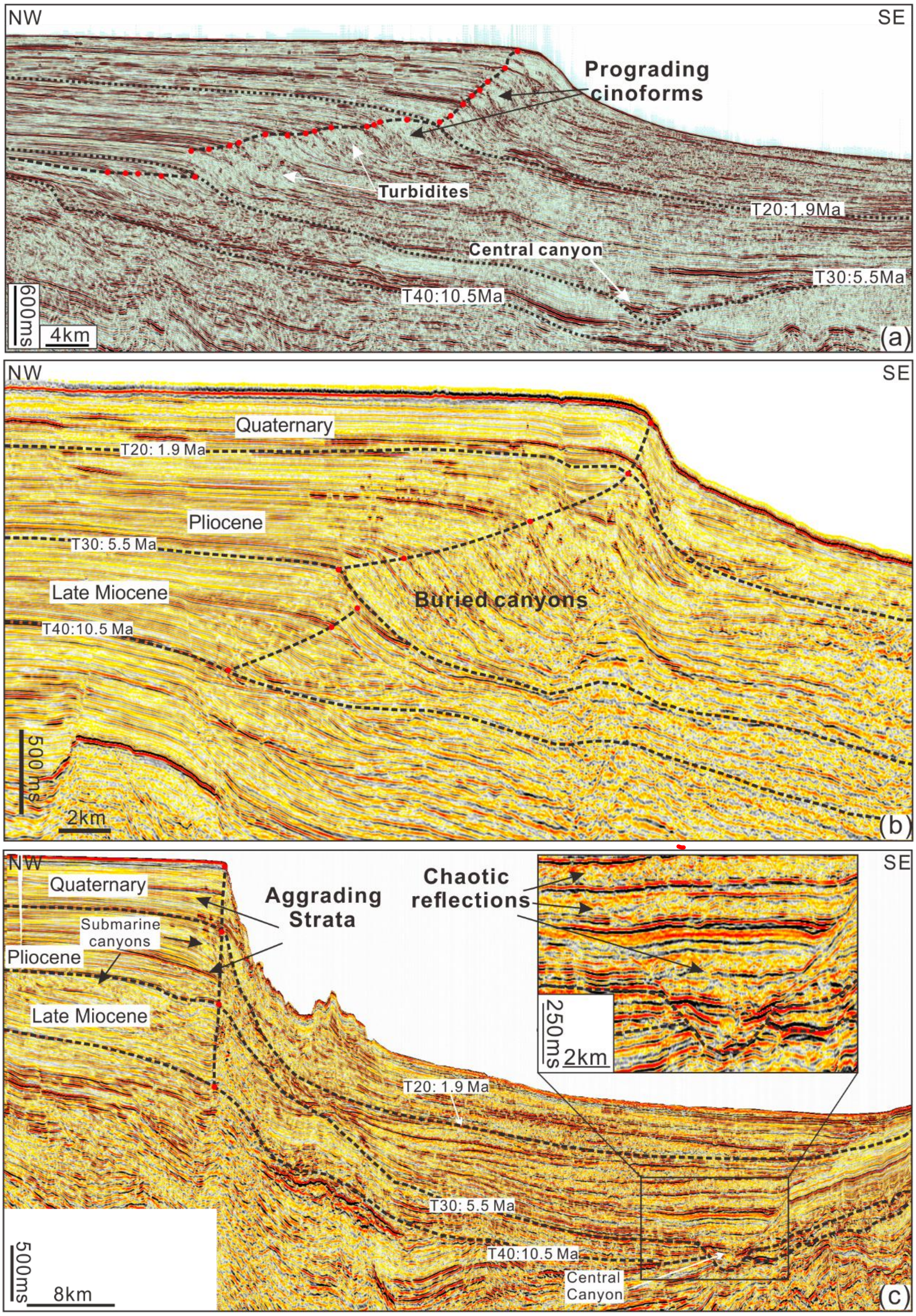

Fig. 6 Two-dimensional (2D) seismic profiles oriented perpendicularly to the northwest South China Sea margin revealing shelf-edge trajectories and sediment stacking patterns at three differernt locations, which are shown in Figure 2. (a) The shelf-margin architecture in the southwest part exhibits a progradational trend since the start of the Late Miocene

(modified from Gong et al., 2015). (b) In the central part, the continental margin shows a progradational trend in the Late Miocene and Pliocene, but an aggradational trend in the Quaternary. (c) The northeast part of the continental margin displays an aggradational trend since the start of the Late Miocene. The red dots in Figure 6a, b and c represent the shelf-edge trajectories.

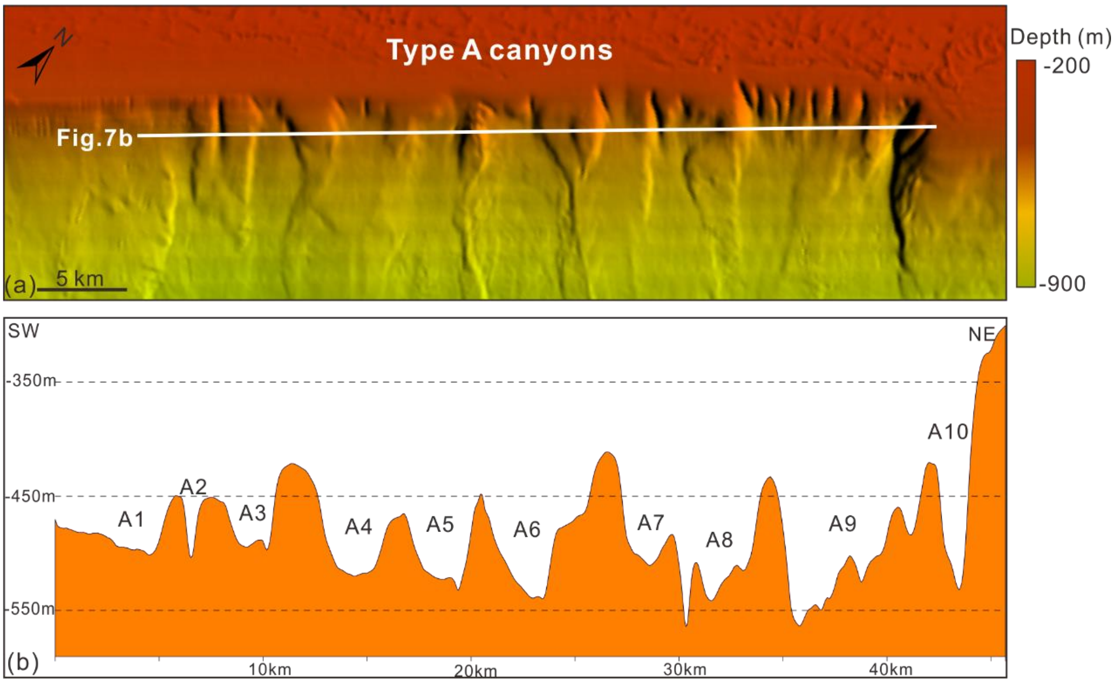

Fig. 7 (a) Multibeam bathymetric map showing the detailed morphology of Type A canyons. The white line marks the bathymetric profile of Type A canyons shown in (b). (b) Bathymetric profile showing the detailed morphological characteristics of Type A canyons. Ten submarine canyons (A1-A10) are observed from southwest to northeast. The length of these canyons varies from 10 to 15 km and their width ranges from 2 to 4 km. The depth of incision of Type A canyons ranges from 40 to 120 m. The slope gradient of Type A canyon walls ranges from 2.4° to 8° on average.

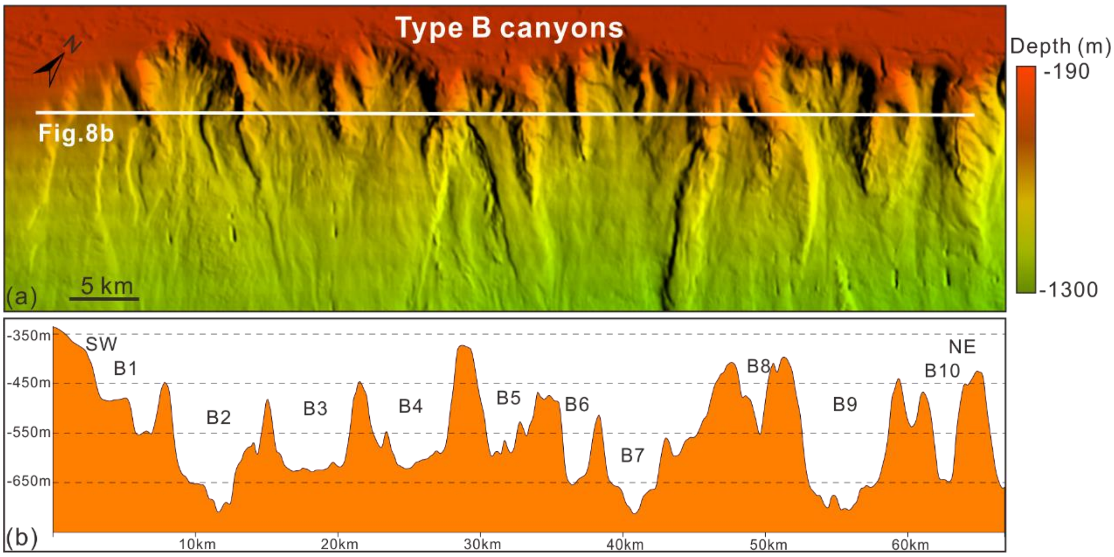

Fig. 8 (a) Detailed morphology of Type B canyons as revealed on bathymetric data. White line represents the bathymetric profile of Type B canyons. Amphitheater-shaped depressions are observed in the canyon heads from west to east. (b) Bathymetric profile showing the geometry of Type B canyons. These canyons have lengths of 15-20 km and widths of 2.5-7.5 km. The depth of incision of Type B canyons ranges from 120 to 240 m. The slope gradient of canyon walls ranges from 4.8° to 8.4° on average.

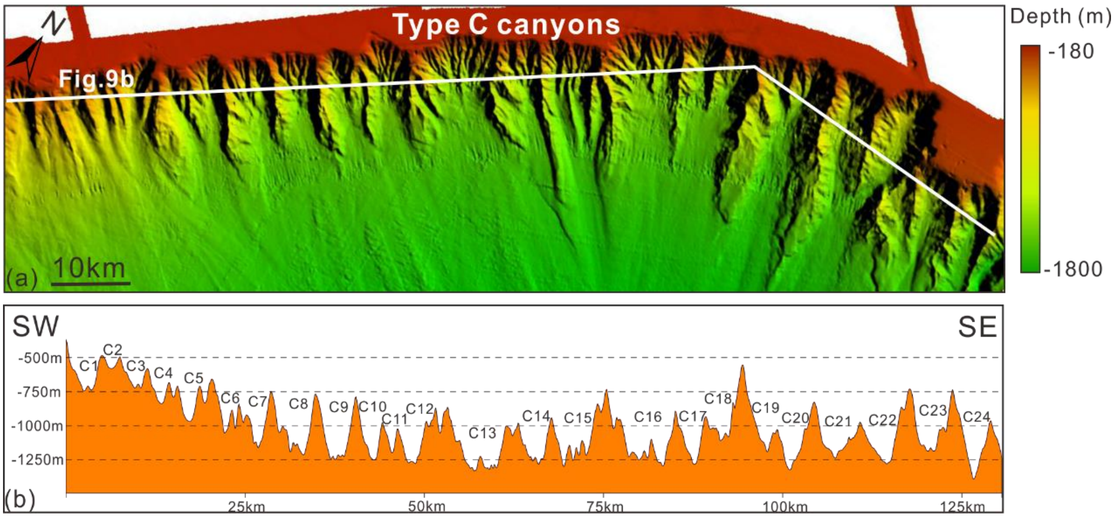

Fig. 9 (a) Bathymetric map highlighting the morphology of Type C canyons. White line represents the bathymetric profile of Type C canyons as shown in (b). (b) Bathymetric profile revealing the geometry of twenty-four Type C canyons. Their lengths range from 15 to 30 km and their widths vary from 5 to 10 km. The depth of incision of Type C canyons ranges from 150 to 450 m. The slope gradient of canyon flanks ranges from 8.5° to 14.8° on average.

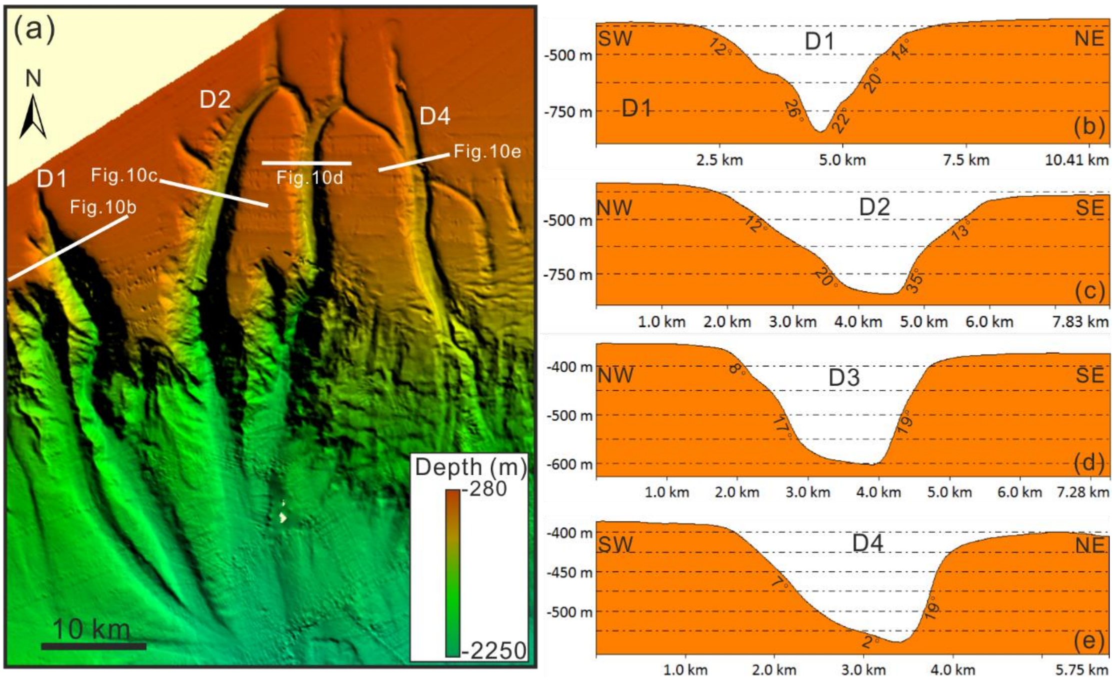

Fig. 10 (a) Bathymetric map revealing the morphology of Type D canyons. Elongated headscarps can be observed in the the heads of Type D canyons. White lines mark the bathymetric profile of four submarine canyons shown in (b), (c), (d) and (e). (b) Bathymetric profile of canyon D1. (c) Bathymetric profile of canyon D2. (d) Bathymetric profile of canyon D3. (e) Bathymetric profile of canyon D4. The lengths of D1 to D4 are 45, 60, 50 and 45 km, respectively. The depth of incision of four Type D canyons ranges from 170 to 580 m. The slope gradient flanks ranges from 4.5° to 24° on average in canyons D1 to D4.

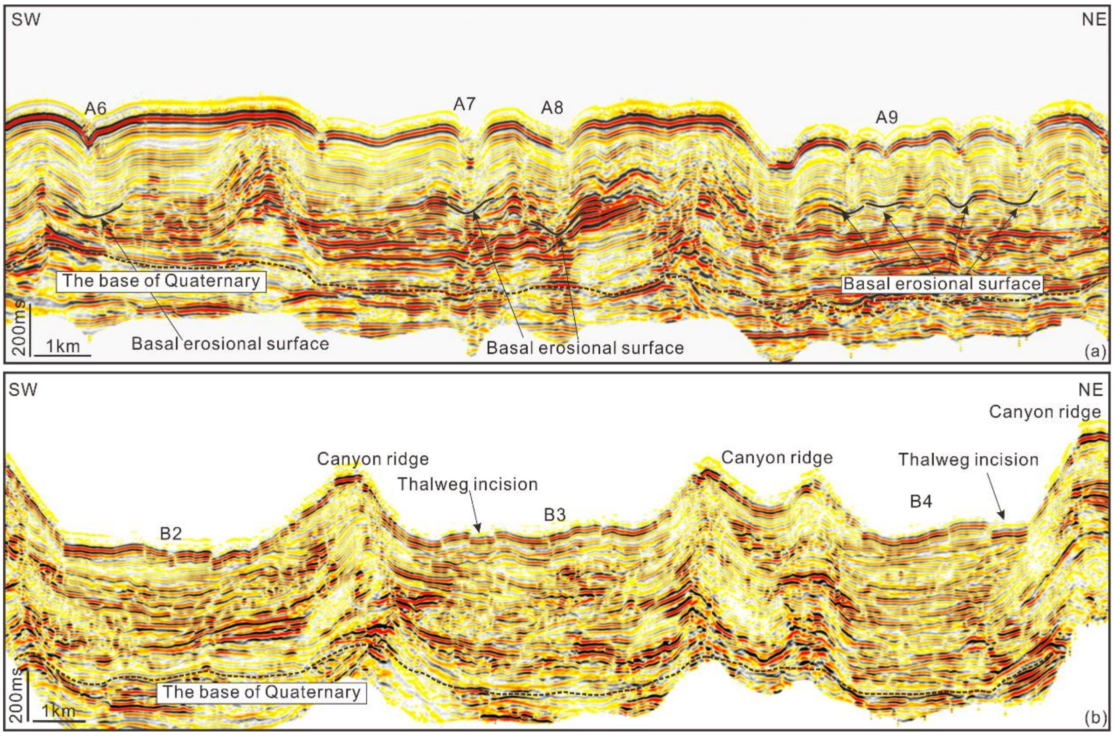

Fig. 11 (a) Two-dimensional (2D) seimsic profile parallel to the shelf break (see location in Figure 2) showing the internal archticture surface of Type A canyons (A6-A9). The black lines mark the basal erosional surface of canyons (b) Two-dimensional (2D) seismic profiles parallel to the shelf break (see location in Figure 2) showing the internal architecture of Type B canyons (B2-B4).

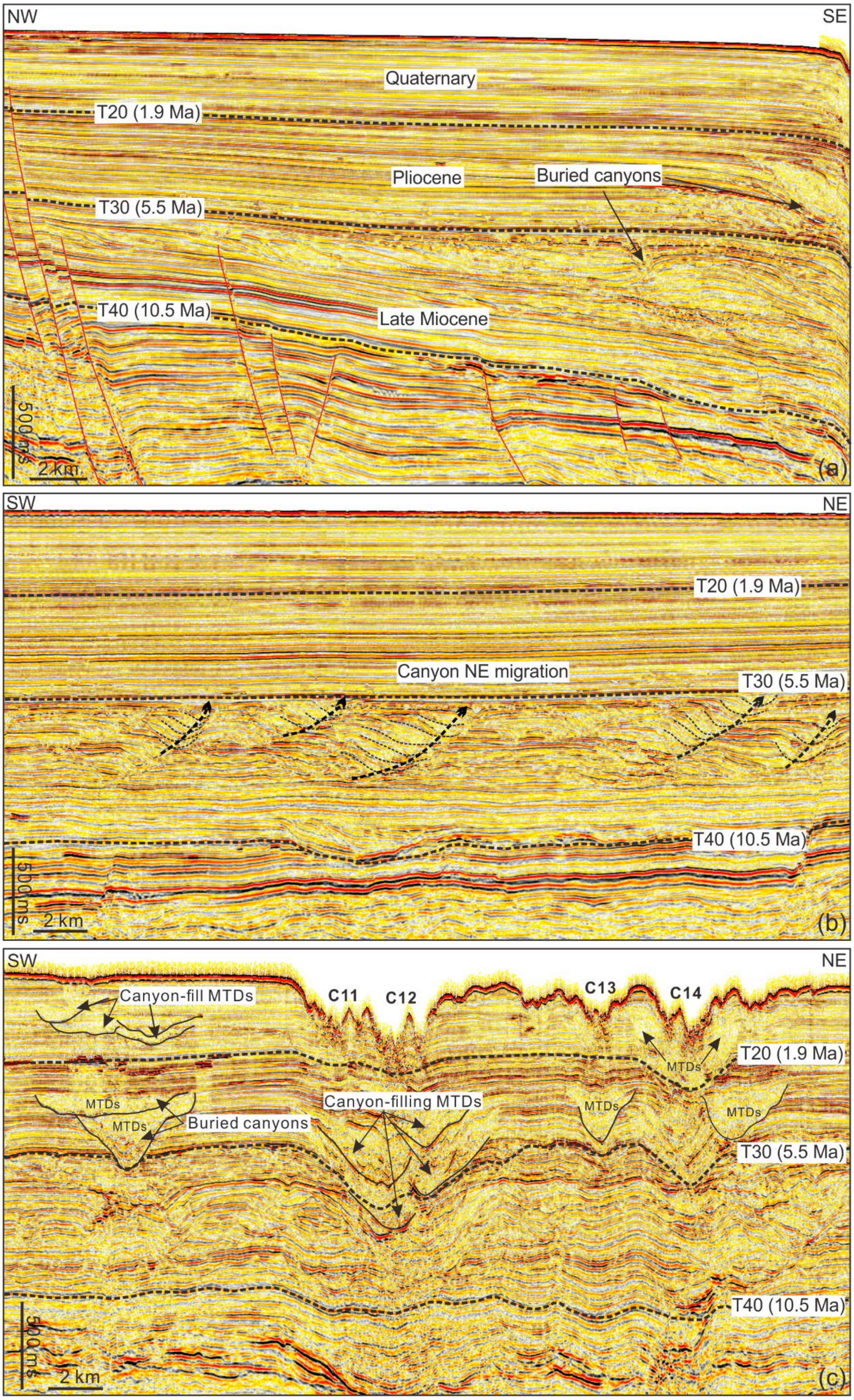

636

637 Fig. 12 (a) Two-dimensional (2D) seismic profile perpendicular to the shelf break showing the evolution of the Type C

canyons since the Late Miocene. The red solid lines represent several normal faults. (b) 2D seismic line perpendicular to the canyon head revealing the development of the canyons. The canyons show a NE migration trend. The erosional surface of canyons is located between Horizons T40 and T30. (c) 2D seismic profile further downslope from b) highlighting the stacking geometries of the canyons. The canyons have a vertical trend and were filled by MTDs. The modern canyons display numerous gullies.

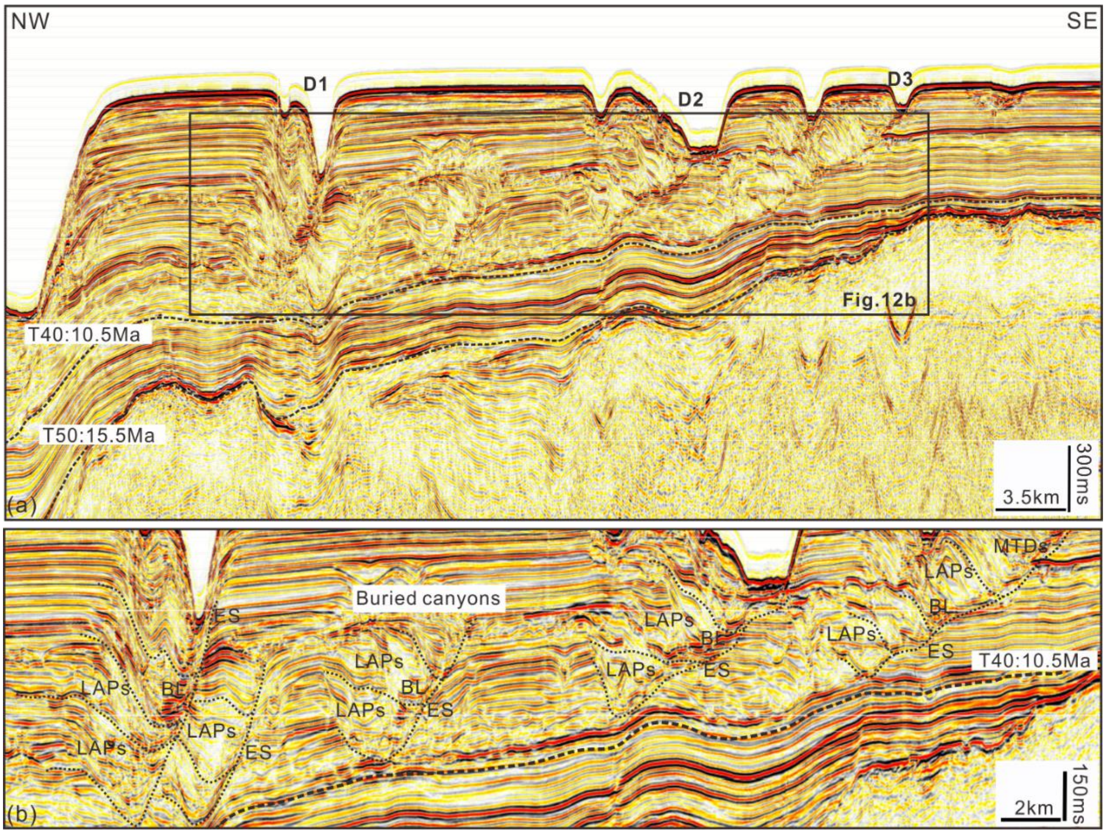

Fig. 13 (a) Two-dimensional (2D) seismic line parallel with the continental slope revealing the development of the Type D canyons since the Late Miocene. (b) Detailed features of seismic facies in the canyons, and their interpretation along the strike direction of the continental slope. The canyons show a NE migration trend. BL: basal lag; LAPs: lateral accretion packages; MTDs: mass transport deposits; ES: erosional surface.